Supporting information for

Comprehensive crystallization retardation of inorganic perovskite for high performance inverted solar cells

Zezhang Wang[1], Tianfei Xu[1], Nan Li[1], Zhen Chang[1], Jing Shan[1], Yong Wang[1], Minfang Wu[1], Fengwei Xiao[1], Shengzhong Liu[2,3,4*], Wanchun Xiang[1,*]

[1]Key Laboratory of Applied Surface and Colloid Chemistry, Ministry of Education, Shaanxi Key Laboratory for Advanced Energy Devices, Shaanxi Engineering Lab for Advanced Energy Technology, School of Materials Science and Engineering, Shaanxi Normal University, Xi'an, 710119, China. wanchun.xiang@snnu.edu.cn

[2]Key Laboratory of Photoelectric Conversion and Utilization of Solar Energy, Dalian Institute of Chemical Physics, Chinese Academy of Sciences, Dalian, 116023, Liaoning, China. szliu@dicp.ac.cn

[3]Center of Materials Science and Optoelectronics Engineering, University of Chinese Academy of Sciences, Beijing, 100049, P. R. China

[4]CNNP Optoelectronics Technology, 2828 Canghai Road, Lingang, Shanghai, China

Experiment

Materials

The F-doped tin oxide (FTO, square resistance is 8-15 Ω cm^{-2}) glass was obtained from Suzhou Shangyang Technology. The Acrylonitrile-methyl acrylate copolymer (AMAC, acrylonitrile ~ 94 wt.%) were obtained from Sigma-Aldrich. 2,2',7,7'-Tetrakis [N, N-di(4-methoxyphenyl)amino]-9,9'-spirobifluorene (Spiro-OMeTAD, 99.8%), lead iodide (PbI_2, 99.99%) and [6,6]-phenyl-C61-butyric acid methyl ester (PC61BM) were obtained from Advanced Election Technology Co. Ltd. [2-(3,6-Dimethoxy-9H-carbazol-9-yl)ethyl]phosphonic acid (MeO-2PACz, SAM) and bathocuproine (BCP) were obtained from Thermo Fisher Scientific. Lead bromide ($PbBr_2$, 99.99%) was purchased from Borun New Material Technology Ltd. Cesium iodide (CsI, 99.99%) and dimethylamine-lead triiodide ($DMAPbI_3$, 99%) was obtained from Xi'an Yuri Solar Co., Ltd. Lithium bis (trifluoromethanesulfonimide) (LiTFSI, 99.0%) was obtained from ACROS Organics. N, N-dimethylformamide (DMF, ≥99.8%), Dimethyl sulfoxide (DMSO, ≥99.9%), chlorobenzene (CB, ≥99%) and 4-tert-butylpyridine (tBP) were obtained from Sigma-Aldrich. Isopropanol (IPA, ≥99.7%) was obtained from Chinese National Pharmaceutical Group Corporation.

The NiO nanoparticles were synthesized based on the procedure reported by Zhang et al.[1] The specific synthesis was carried out by dissolving 9 g of nickel (II) nitrate hexahydrate in 150 mL of deionised water and stirring at room temperature to obtain a clear green solution. Next, sodium hydroxide solution was added to the solution until the pH reached ~10, and then the mixture was stirred for 30 min. the resulting colloid was washed twice with deionised water and dried at 80 °C overnight. Finally, the obtained green powder was calcined at 275°C for 2h to form a deep black powder.

Device fabrication

p-i-n $CsPbI_{3-x}Br_x$ PSCs:

FTO/glass was cleaned with detergent, deionized water, acetone and ethanol in an ultrasonic bath for 30 min sequentially, dried with compressed nitrogen flow. Before use, the FTO/glass was treated with plasma for 15 min. NiO_x nanoparticle solution (10 mg mL^{-1} in deionized water) was spun onto

FTO/glass at 4000 rpm for 30 s, followed by annealing in air at 150 °C for 20 min and then transferred into air glovebox. SAM (10 mg mL^{-1} in IPA) layer was deposited on NiO_x surface at 3000 rpm for 30 s and annealing at 100 °C for 10 min. Perovskite layer was prepared by spinning solution of $CsPbI_{3-x}Br_x$ perovskite precursor (CsI, $DMAPbI_3$, and $PbBr_2$ at a 3.00: 2.85: 0.15 molar ratio in DMF/DMSO mixed solvent (V_{DMF}: V_{DMSO}= 8.5:1.5)) on SAM layer at 1000 rpm for 10 s and 4000 rpm for 40 s, followed by annealing at 210 °C for 5 min. AMAC-incorporated perovskite layer was prepared by spinning solution of AMAC-$CsPbI_{3-x}Br_x$ perovskite precursor (AMAC amounts were: 0.1, 0.3, 0.6 mg mL^{-1}) on SAM at 1000 rpm for 10 s and 4000 rpm for 40 s, followed by annealing at 210 °C for 8 min. The prepared perovskite film was quickly transferred into air glovebox. PCBM (20 mg mL^{-1} in CB) layer was spun on the perovskite film surface at 2000 rpm for 30 s. BCP (1 mg mL^{-1} in IPA) layer was dynamically spun on PCBM surface at 5000 rpm for 30 s. Finally, 90 nm thick silver electrode was thermally evaporated on BCP. All the above operations were carried out at RH~20%.

n-i-p $CsPbI_{3-x}Br_x$ PSCs:

Glass cleaning and plasma treatment consistent with p-i-n PSCs. Preparation of TiO_2 electron transport layer on FTO/glass substrate by chemical deposition. The dense TiO_2 layer was deposited by heating an aqueous solution of 40 mM $TiCl_4$ at 70 °C for 60 min. The TiO_2/FTO/glass substrate was then annealed at 200°C for 30 minutes, cooled to room temperature and plasma treated for five minutes before being transferred to a nitrogen-filled glove box. Perovskite layer was prepared by spinning solution of $CsPbI_{3-x}Br_x$ perovskite precursor on TiO_2 layer at 1000 rpm for 10 s and 4000 rpm for 30 s, followed by annealing in air at 210 °C for 8 min. For the hole transport layer, the Spiro-OMeTAD solution (90 mg Spiro-OMeTAD, 36 μL of tBP, and 22 μL of LiTFSI (520 mg mL-1 in acetonitrile) were dissolved in 1 mL of CB.) was spin-coated on the perovskite surface at 5000 rpm for 30 s. After 10 h of oxidation, 90 nm gold electrodes were thermally evaporated onto the surface of the Spiro-OMeTAD using a mask plate with an active area of 0.09 cm^2.

DFT calculations

All calculations are performed by the spin unrestricted DFT method as implemented in DMol3 code of the Materials Studio package.[1] The electron exchange and correlation effect are described by the generalized gradient approximation (GGA) based on the Perdew-Burke-Ernzerhof (PBE), and double numerical plus polarization (DNP) basis set is adopted.[2] A smearing value of 0.005 Ha to the orbital occupation is employed for all calculations. The convergence tolerance for energy change, max force, and max displacement are 2.0 × 10^{-5} Ha, 0.004 Ha $Å^{-1}$, and 0.005 Å, respectively.

The Interaction energy of the molecules is defined as:

$$E_{Int} = E_{*M} - E_{*} - E_{M} \quad (1)$$

where E*M, E*, and EM represent the energies of Structure AMAC adsorbed with molecule, isolated Structure AMAC, and molecule, respectively.

Solution characterizations:

The viscosity data were obtained from a viscometer (DV3TLVTJ0 150VA) by Brookfield, USA (the test temperature is 25°C). The size distribution of the perovskite-solvent complexes in the

precursor solution was obtained using a Brookhaven laser particle sizer (90Plus, the solvent is DMF and the test temperature is 20±5°C).

Film characterizations:

The X-ray photoelectron spectroscopy (XPS) spectra and the ultraviolet photoelectron spectroscopy (UPS) spectra were collected on monochromatized Al K-alpha targets using an X-ray photoelectron spectrometer (Escalab Xi+) manufactured by Thermo Fisher Scientific. The Fourier-transform infrared (FTIR) spectra were collected using a VERTEX 70 FTIR spectrometer by Brooke Germany. The surface morphology of the perovskite images was obtained using SU-8020 field emission swept surface electron microscope (SEM) by HATACHI. In-situ PL spectra was recorded by a QE-Pro (Ocean Optics) spectrometer. The atomic force microscope (AFM) and Kelvin probe microscopy (KPFM) images were obtained using Dimension Icon four-probe setup by BRUKER. The Steady-state photoluminescence (PL), time-resolved photoluminescence (TRPL) and PL-mapping images were obtained using PicoQuant 300 time-resolved spectroscopy (PicoQuant) with an excitation wavelength of 510 nm. The ultraviolet visible (UV–vis) absorption spectra were obtained using UV-3600 UV-visible spectrophotometer by Shimadzu. The X-ray diffraction (XRD) and grazing incidence XRD (GIXRD) were obtained using SmartLab high resolution X-ray diffractometer by JEOL Japan Electronics Co., Ltd. The transmission electron microscope (TEM) patterns were obtained using JEM-2800 Field emission ultra-high resolution transmission electron microscope by JEOL Japan Electronics Co., Ltd. Ambient stability test of perovskite films was performed at relative humidity (RH) of 20-30%. In-situ X-ray diffraction (in-situ XRD) was obtained by annealing at 210 °C on a SmartLab high resolution X-ray diffractometer from JEOL Nippon Electronics Co.

Device characterizations:

The *J-V* characteristic curves of PSCs were measured from Enlitech's SS-F5-3A solar simulator under 100 mW cm-2 illumination. The simulator was calibrated for light intensity using an NREL traceable KG5 filtered silicon reference cell, with the device area defined by a metal mask with an aperture area of 0.09 cm^2. The external quantum efficiency (EQE) of the device was measured using the ESB-6 QTest Station 500TI system from Enlitech Technology Co. Stable output power (SPO) of the device was obtained on Crowntech's QTest Station 2000 ADI system. Measurement of space charge limiting current (SCLC) in FTO/NiO_x/perovskite (with or without AMAC)/spiro-OMeTAD/Au devices in the dark. Capacitance-voltage (*C-V*) and electrochemical impedance spectroscopy (EIS) measurements were performed on the devices on a Zahner Zennium electrochemical workstation (AMETEK-Modulab XM, USA). *J-V* curve measurements were performed on the device in a dark environment to obtain dark state *J-V* characteristics. The correlation between V_{OC} and light was obtained from *J-V* curves at different light intensities. The ion migration activation energy was evaluated on CGO-4 temperature-dependent vaccum probe setup by Cindbest (China) with the device structure of FTO/perovskite(with or without AMAC)/Au. The device ambient stability was tested by storing devices in an environment with RH of 20-30%. The operational stability tests were performed on unencapsulated inorganic PSCs under continuous tracking at the maximum power point (MPP) using a 1-sun equivalent white-light LED array. The MPP tests were conducted at 35 °C in RH~10% atmosphere with 10 min interval (Multi-Channels

Solar Cells Stability Test System, Wuhan 91PVK Solar Technology Co. Ltd, China). The time-of-flight secondary ion mass spectrometry (TOF-SIMS) was measured using an ION ToF-SIMS 5 by ION-TOF GmbH. For detection of negative and positive ions, Cs^{+} and O^{2-} ions were used with 1 keV ion energy. Femtosecond transient absorption spectra (F-TAS) were obtained from a commercial TA system using an excitation wavelength of 550. This was built with a high-speed spectrometer (Ultrafast systems, HELIOS) and a regenerative amplified Ti:Sapphire laser (light conversion, 1030 nm, 150 fs, 100 kHz repetition).

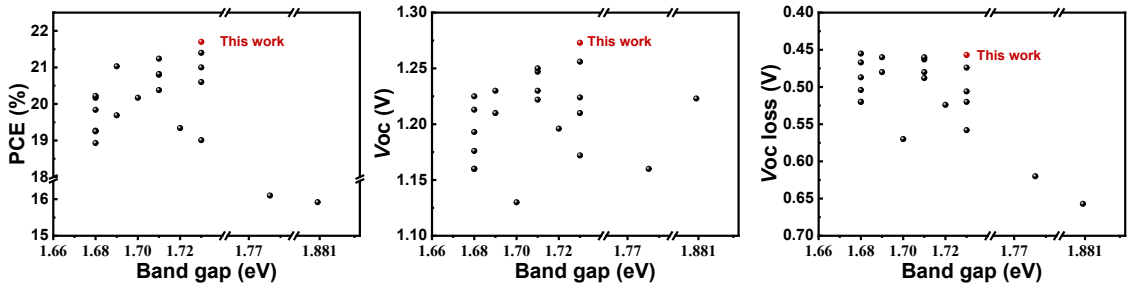

Fig. S1 Representative PCE, V_{OC} and V_{OC} loss of inverted structure inorganic PSCs collected from recent publications (ref.1-22, the detailed PV parameters are shown in **Table S1**).

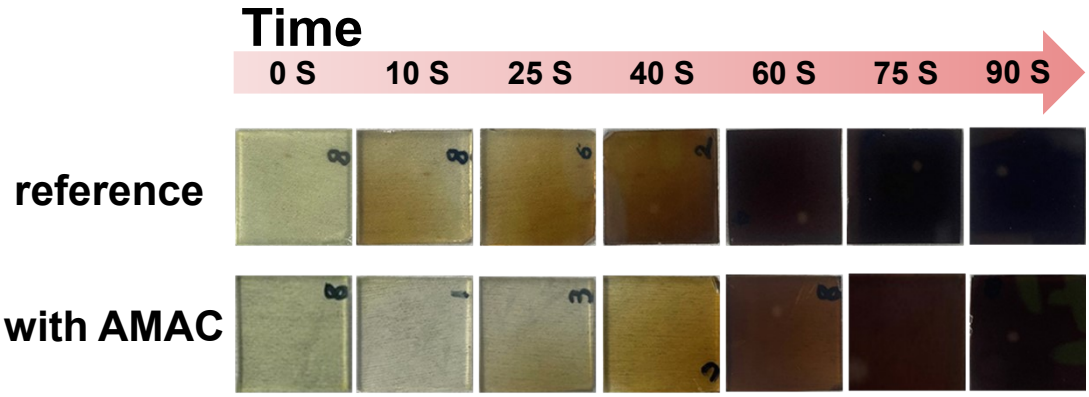

Fig. S2 Photographs of films annealed at 210 °C for various time.

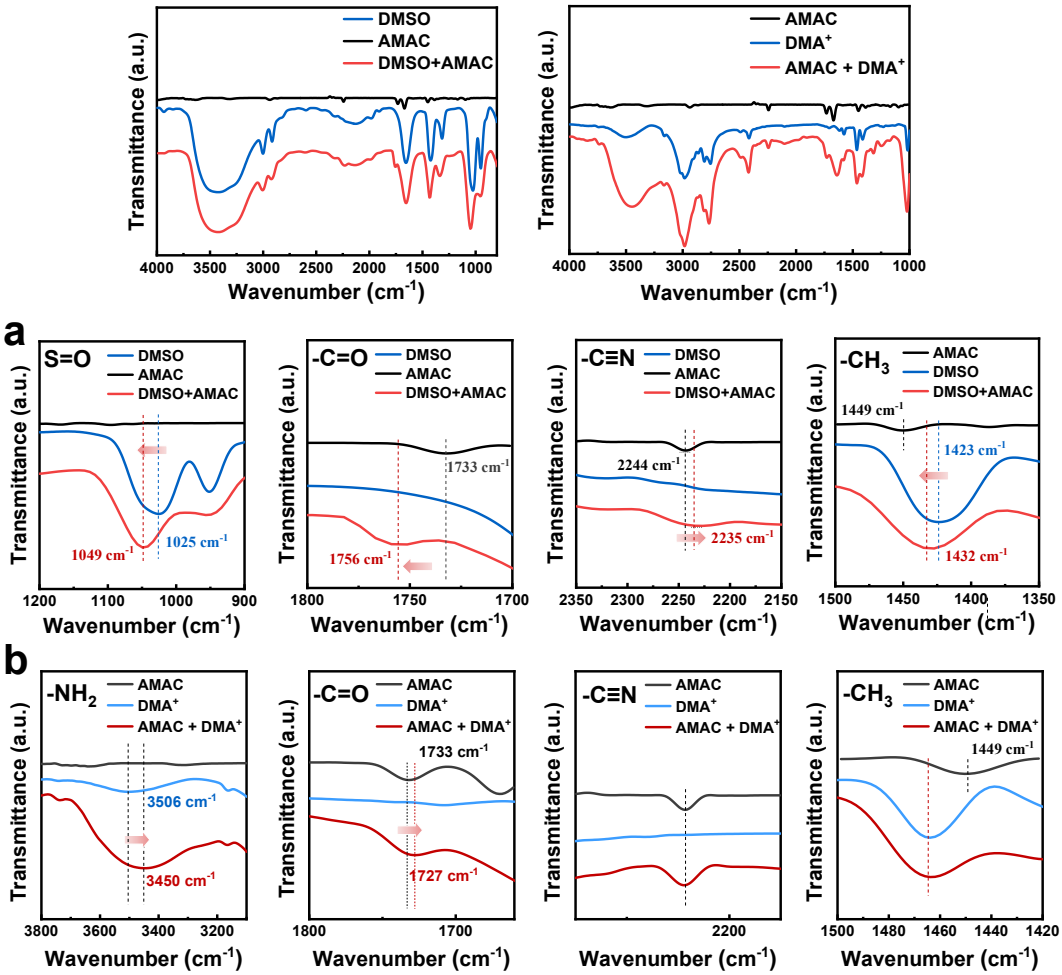

Fig. S3 FTIR spectra of (**a**) AMAC, DMSO, AMAC-DMSO and (**b**) AMAC, DMA^+, AMAC-DMA^+ samples.

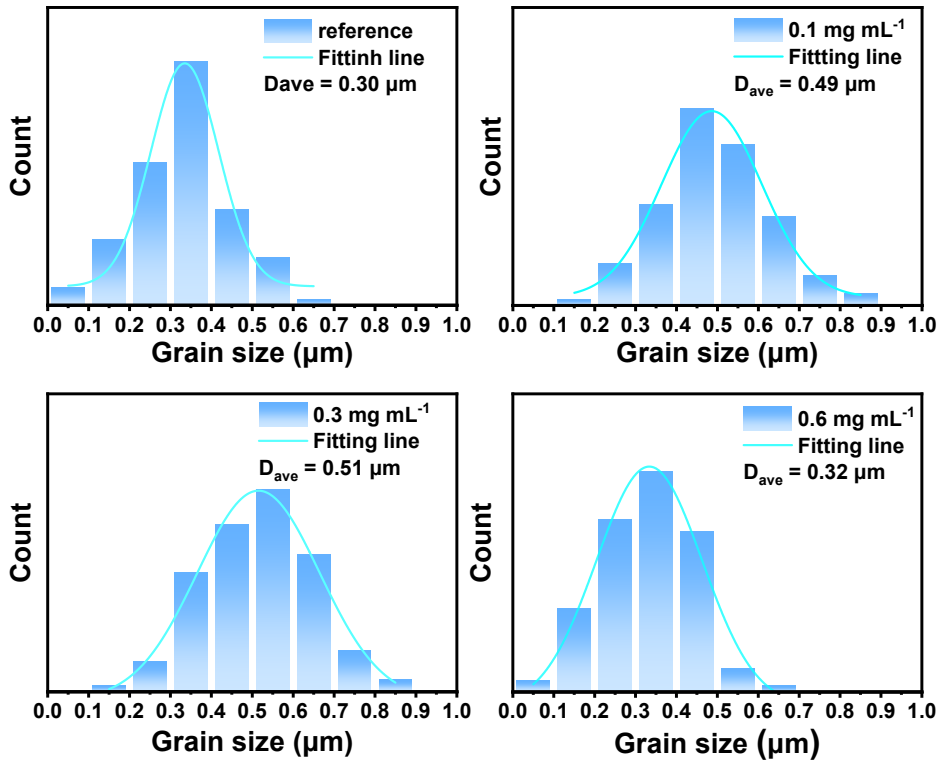

Fig. S4 Grain statistics of perovskite incorporated with different AMAC concentrations.

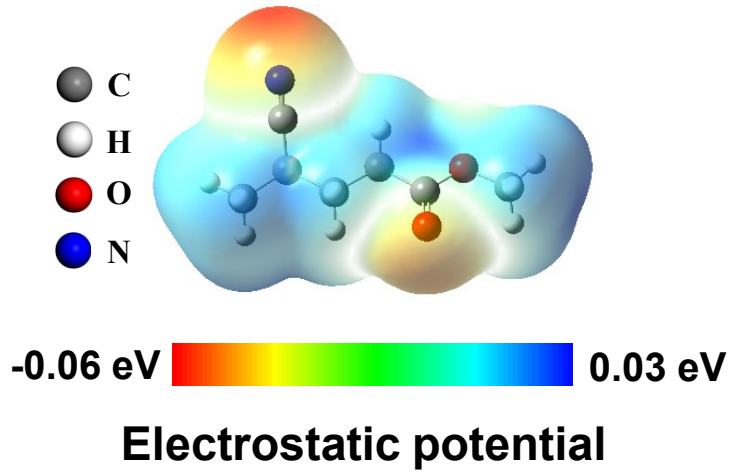

Fig. S5 RSP analysis of molecular formula of AMAC monomer.

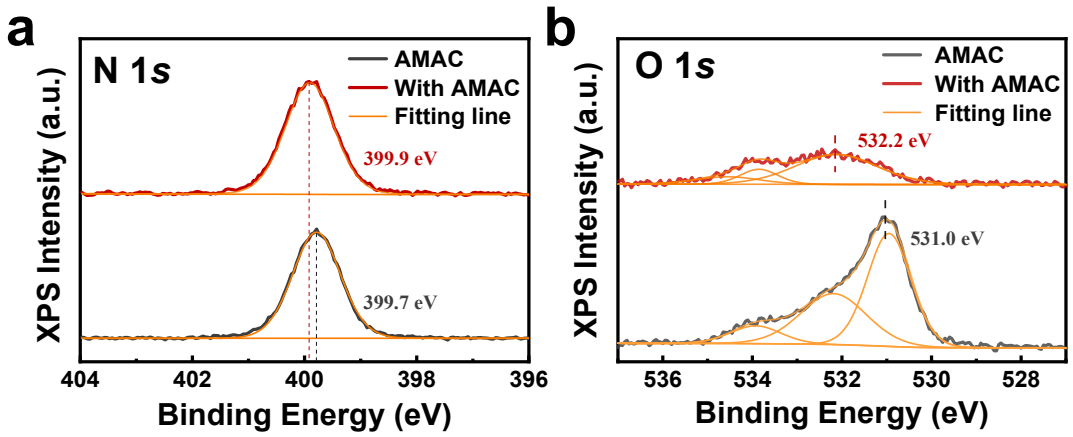

Fig. S6 XPS spectra of (**a**) N 1*s* and (**b**) O1*s* from AMAC and perovskite film with AMAC incorporation.

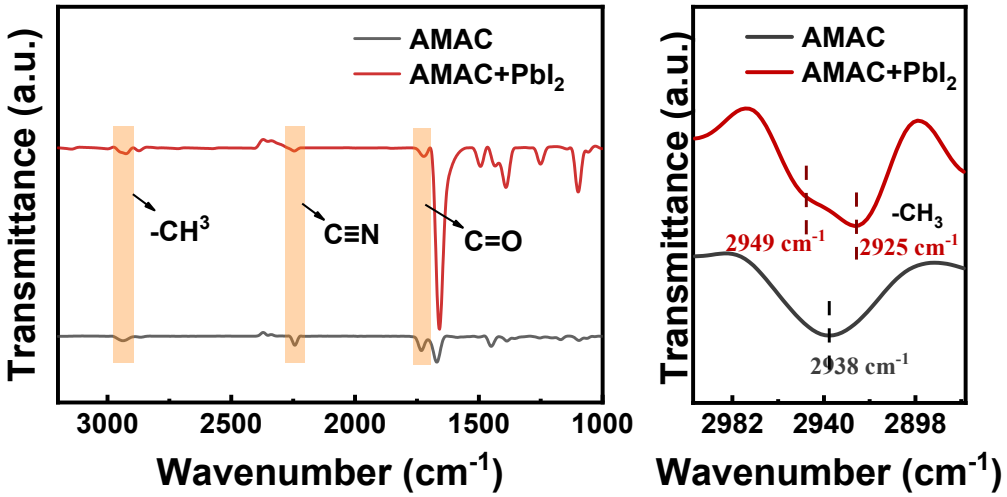

Fig. S7 FTIR spectra of AMAC and AMAC-PbI_2 films.

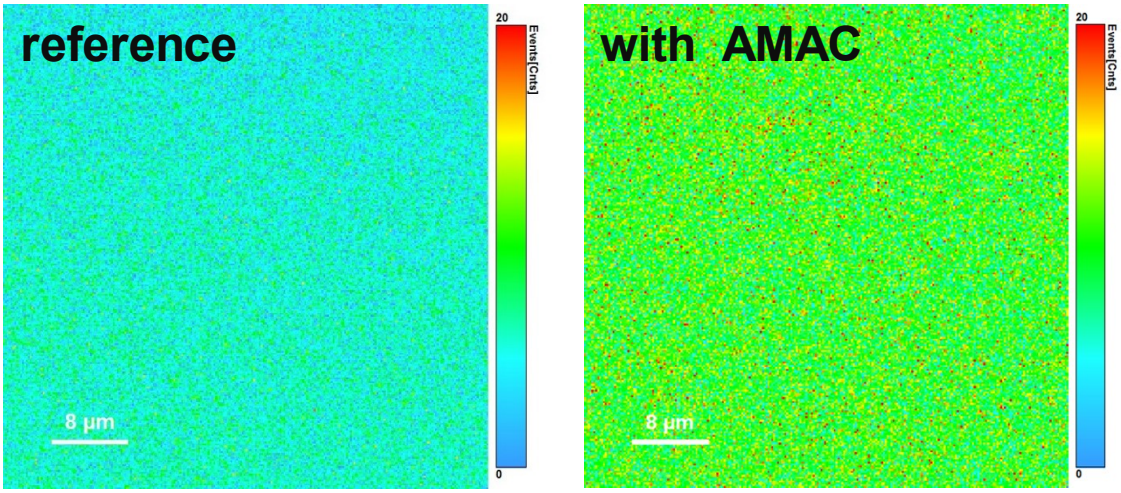

Fig. S8 PL-mapping images of inorganic perovskite thin films with and without AMAC incorporation.

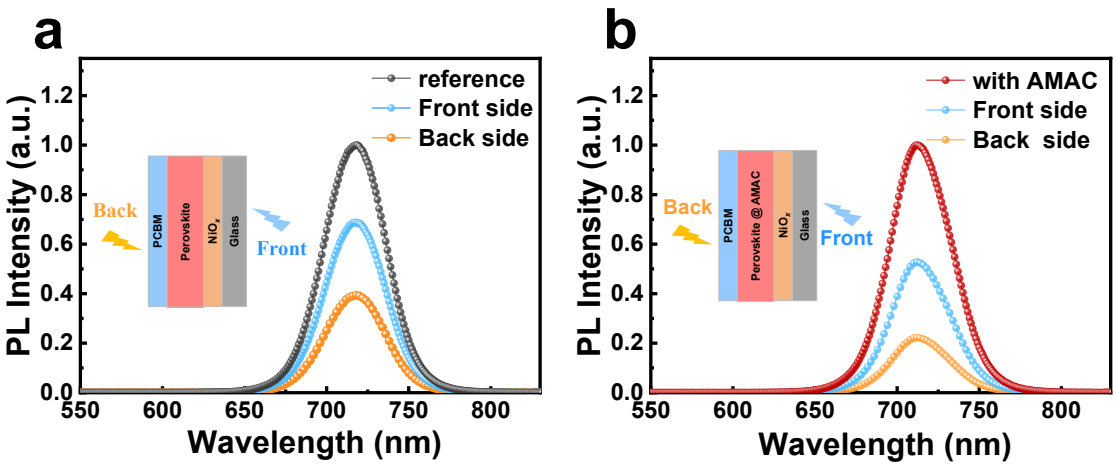

Fig. S9 Steady-state photoluminescence (PL) properties of stacked samples (a) without and (b) with AMAC incorporation. Stacked samples are structured as Glass/NiO_x/perovskite (with or without AMAC)/PCBM.

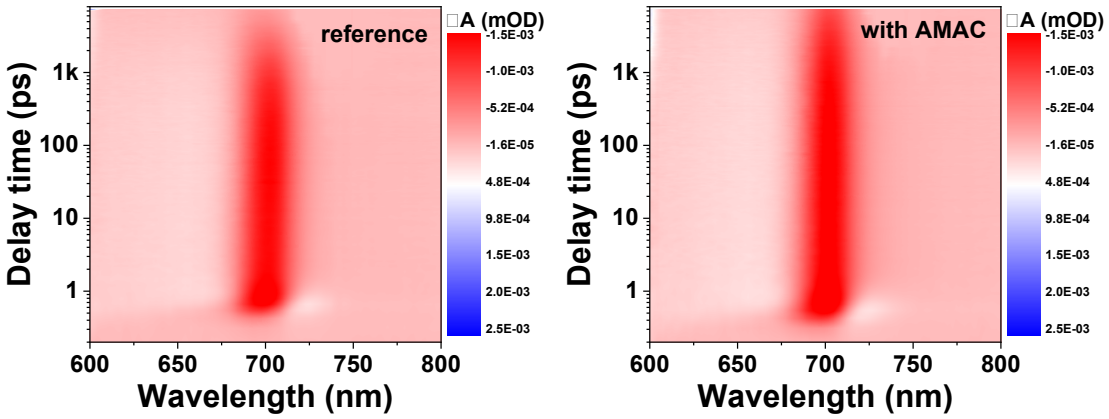

Fig. S10 The 2D contour plot of TAS of the photoinduced absorption as a function of wavelength and delay time for perovskite films with and without AMAC incorporation.

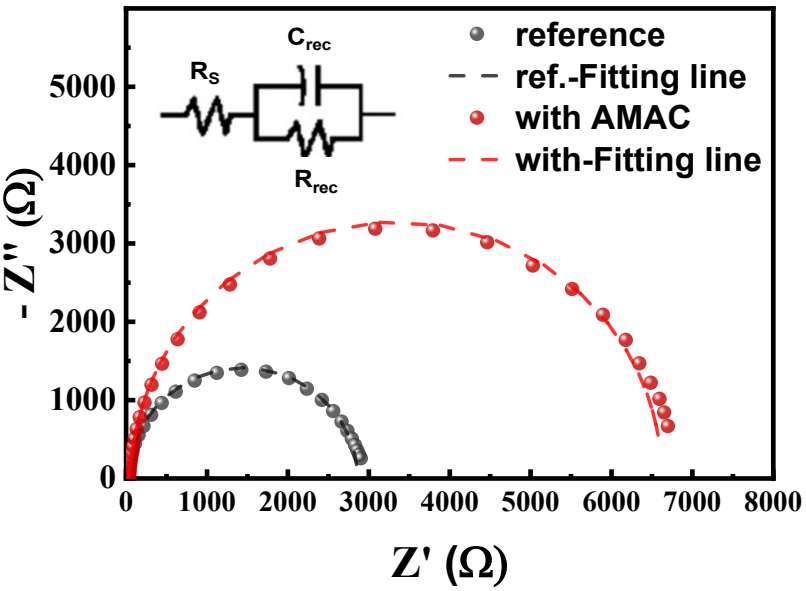

Fig. S11 EIS curves of devices with and without AMAC incorporation.

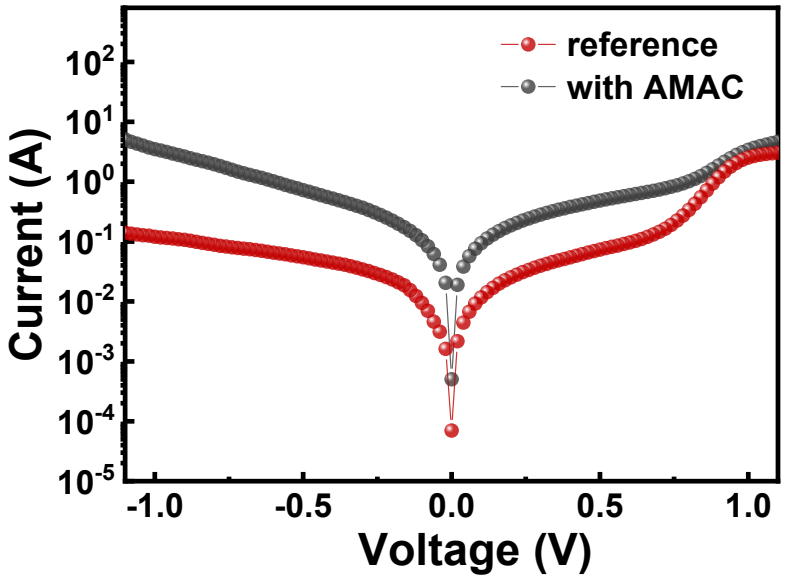

Fig. S12 Dark *J-V* curves of devices with and without AMAC incorporation.

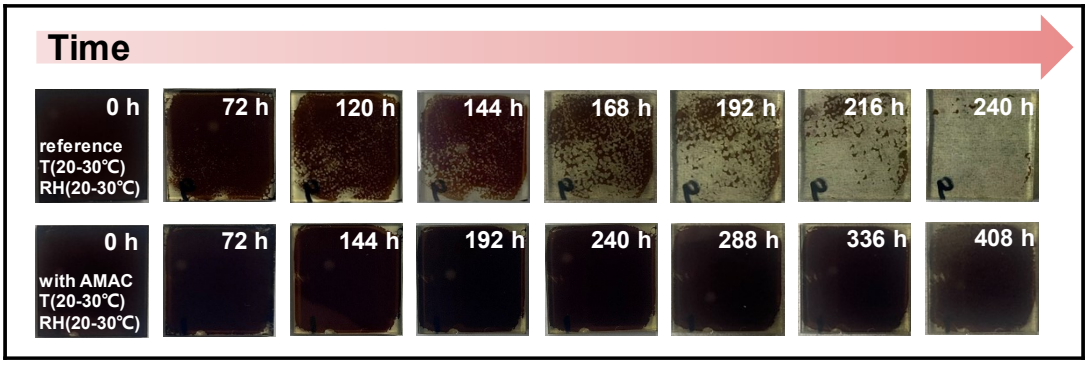

Fig. S13 Photographs of the decomposition of inorganic perovskite films with and without AMAC incorporation, stored at RH 20%-30%.

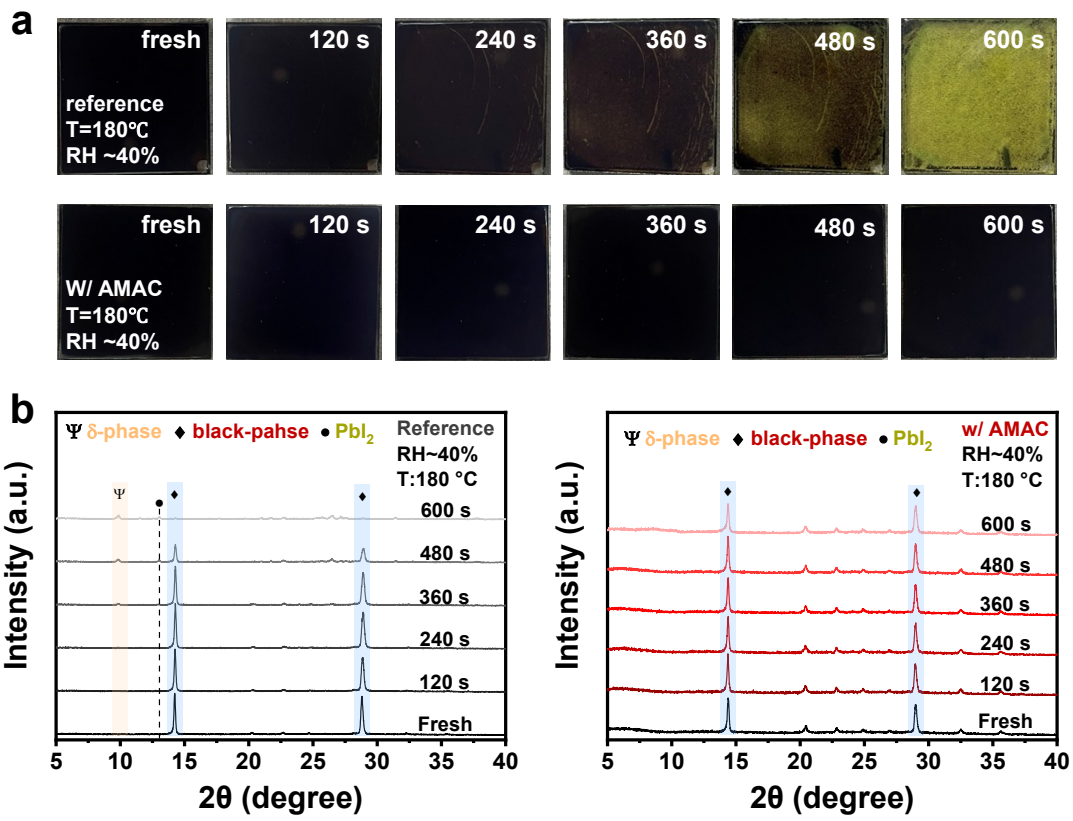

Fig. S14 (**a**), Photographs and (**b**), XRD patterns of decomposition of inorganic perovskite films with and without AMAC at 180 °C and ~40% relative humidity.

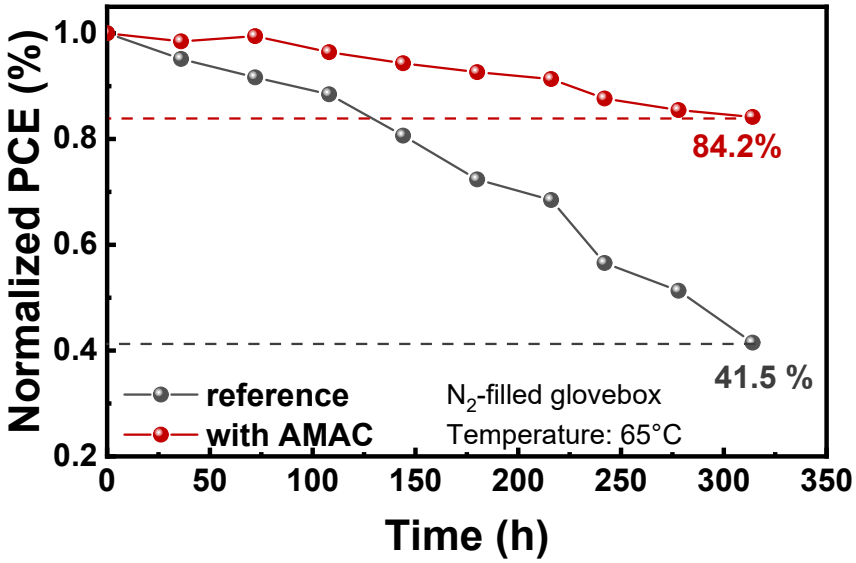

Fig. S15 Thermal stability of inorganic PSCs under 65 °C aging in a N_2 glovebox without encapsulation.

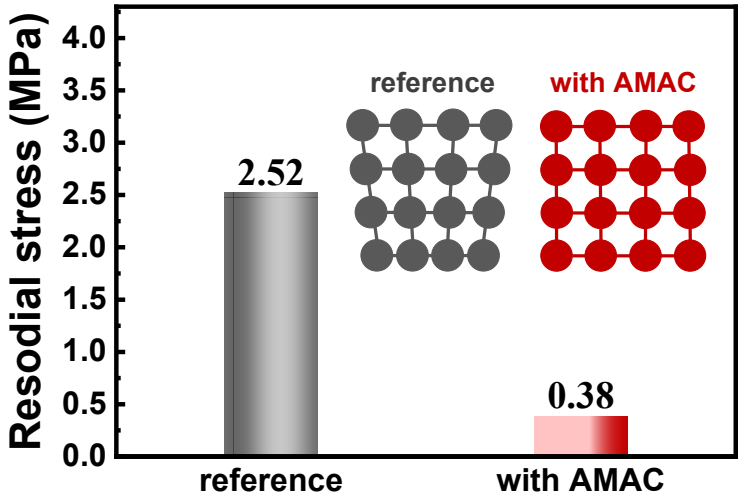

Fig. S16 Residual stress within perovskite films.

Table S1. Summary of device structures and photovoltaic parameters of inverted inorganic PSCs from literature.

Device structure	Eg (eV)	V_{OC} (V)	J_{SC} (mA cm^{-2})	FF (%)	PCE (%)	ref.
ITO/P3CT-N/$CsPbI_3$/DAB/PCBM/C_{60}/BCP/Ag	1.68	1.213	20.35	80.37	19.84	3
FTO/P3CT/$CsPbI_3$/PACl/PCBM/BCP/Ag	1.70	1.130	21.36	84.0	20.17	4
ITO/MeO-2PACz/γ-CsPbI3/β-CsPbI3/PCBM/BCP/Ag	1.68	1.16	20.64	84.17	20.17	5
ITO/P3CT-N/$CsPbI_2Br$/FABr/PCBM/C_{60}/BCP/Ag	1.88	1.223	16.35	16.35	15.92	6
ITO/NiO_x/$CsPbI_xBr_{3-x}$/6TIC-4F/ZnO/C_{60}/Ag	1.78	1.16	17.7	78.60	16.1	7
ITO/PTAA/$CsPbI_3$/OMXene-$CsPbI_3$/CPTA/BCP/Ag	1.69	1.21	19.86	81.96	19.69	8
FTO/NiO_x/$CsPbI_xBr_{3-x}$/MMI/PCBM/BCP/Ag	1.73	1.21	20.33	83.6	20.6	9
ITO/NiO_x/$CsPbI_{2.85}Br_{0.15}$/ABA/PCBM/BCP/Ag	1.71	1.222	19.92	83.67	20.38	10
ITO/P3CT-N/$CsPbI_3$(FBJ)/PCBM/C_{60}/BCP/Ag	1.68	1.225	20.33	77.37	19.27	11
ITO/NiO_x/$CsPbI_{2.85}Br_{0.15}$/PCBM/BCP/Cu	1.72	1.196	19.30	83.79	19.34	12
ITO/P3CT-N/$CsPbI_3$/MAAC/PCBM/C_{60}/BCP/Ag	1.68	1.160	20.46	81.13	19.25	13
ITO/P3CT-N/$CsPbI_3$-MMDS/PCBM/C_{60}/TPBi/Cu	1.73	1.172	20.58	78.84	19.01	14
ITO/P3CT-N/$CsPbI_3$/Si-Cl/PCBM/C_{60}/BCP/Ag	1.68	1.176	20.10	80.04	18.93	15
ITO/MeO-2PACz/P3CT-N/$CsPbI_3$/4-IEA/PCBM/C_{60}/TPBi/Ag	1.68	1.193	20.68	81.95	20.22	16
FTO/NiO_x/MeO-2PACz/$CsPbIxBr_{3-x}$/MPTS/PCBM/BCP/Ag	1.73	1.224	20.36	84.2	21.0	17
ITO/NiO_x/$CsPbI_{2.85}Br_{0.15}$(5-MVA)/PCBM/BCP/Ag	1.71	1.23	20.82	84.31	20.05	18
ITO/PTAA/$CsPbI_3$/Cs_4PbBr_6PNCs/CPTA/BCP/Ag	1.69	1.23	21.03	84.79	20.16	19
ITO/NiO_x/P3CT-N/$CsPbI_{2.85}Br_{0.15}$/ABF/PCBM/BCP/Ag	1.71	1.247	19.62	84.97	20.80	20
ITO/NiO_x/MeO-2PACz/NCL/$CsPbI_3$/ABF/PCBM/BCP/Ag	1.71	1.25	20.50	83.1	21.24	21
FTO/NiO_x/MeO-2PACz/$CsPbI_xBr_{3-x}$/YbTFSI/PCBM/BCP/Ag	1.73	1.256	20.38	83.6	21.4	22
FTO/NiO_x/MeO-2PACz/$CsPbIxBr_{3-x}$(AMAC)/PCBM/BCP/Ag	1.73	1.273	20.30	83.9	21.7	This work

Note: Indium-Tin Oxide (ITO) glass; F-doped tin oxide (FTO) glass; Poly[3-(4-carboxylatebutyl)thiophene]–CH_3NH_2 (P3CT-N); Poly[3-(4-carboxylatebutyl)thiophene] (P3CT, Mw: 30-40k); [2-(3,6-Dimethoxy-9H-carbazol-9-yl)ethyl]phosphonic acid (MeO-2PACz); Fullerene C_{60} (C_{60}); Poly(triaryl amine) (PTAA); 1,3,5-tris(1-phenyl-1H-benzimidazol-2-yl)benzene (TPBi); [6,6]-phenyl-C61-butyric acid methyl ester ($PC_{61}BM$); bathocuproine (BCP); 1,4-butanediamine (DAB); propylamine hydrochloride (PACl); formamidinium bromine (FABr); 6TIC-4F is a synthesis of terthieno[3,2-b]thiophene and 2-(5,6-difluoro-3-oxo-2,3-dihydro-1H-inden-1-ylidene)malononitrile; oxidized MXene (OMXene); 2-mercapto-1-methylimidazole (MMI); 2-amino-5-bromobenzamide (ABA); 3, 5-difluorobenzoic acid hydrazide (FBJ); maleic anhydride (MAAD); 4-Imidazoleethylamine (4-IEA); 1,2-bis(chlorodimethylsilyl)ethane (Si–Cl); (3-mercaptopropyl) trimethoxysilane (MPTS); 3-amino-5-bromopyridine-2-formamide (ABF); niobium pentachloride (NCL); Ytterbium(III) trifluoromethanesulfonate (YbTFSI); 5-maleimidovaleric acid (5-MVA); Cs_4PbBr_6 perovskite nanocrystals (PNCs).

Table S2 Hysteresis of the reference and AMAC-incorporated inorganic PSCs. Devices with an active area of 0.09 cm^2 were illuminated under 1 sun irradiation.

devices	V_{OC} (V)	J_{SC} (mA cm^{-2})	FF (%)	PCE (%)	HI (%)
Ref.-RS	1.172	20.30	81.4	19.4	8.2
Ref.-FS	1.100	20.29	79.8	17.8	
w/ AMAC-RS	1.273	20.30	83.9	21.7	4.1
w/ AMAC-FS	1.258	20.29	81.3	20.8	

Table S3 Charge lifetimes in perovskite films with and without AMAC incorporation from TRPL measurement.

	τ_{ave} (ns)	τ_{ave} (ns)	Amplitude τ_1 (%)	τ_2 (ns)	Amplitude τ_2 (%)
reference	66.07	72.34	88.14	19.47	11.86
w/ AMAC	118.02	250.24	33.40	51.72	66.60

Table S4 The fitted EIS parameters of IPSCs with and without AMAC incorporation.

Devices	R_s(Ω)	C_{tr} (F)	R_{rec} (Ω)	C_{rec} (F)
reference	18.5	8.3×10^{-10}	2827	1.41×10^{-8}
w/ AMAC	32.5	1.3×10^{-8}	6551	6.52×10^{-9}

References

1. B. Delley, *The Journal of Chemical Physics*, 2000, **113**, 7756-7764.
2. J. P. Perdew, K. Burke and M. Ernzerhof, *Physical Review Letters*, 1997, **78**, 1396-1396.
3. S. Fu, J. Le, X. Guo, N. Sun, W. Zhang, W. Song and J. Fang, *Advanced Materials*, 2022, **34**, 2205066.
4. S. Wang, M.-H. Li, Y. Zhang, Y. Jiang, L. Xu, F. Wang and J.-S. Hu, *Energy & Environmental Science*, 2023, **16**, 2572-2578.
5. R. Ji, Z. Zhang, Y. J. Hofstetter, R. Buschbeck, C. Hänisch, F. Paulus and Y. Vaynzof, *Nature Energy*, 2022, **7**, 1170-1179.
6. S. Fu, X. Li, L. Wan, W. Zhang, W. Song and J. Fang, *Nano-Micro Letters*, 2020, **12**, 170.
7. J. Wang, J. Zhang, Y. Zhou, H. Liu, Q. Xue, X. Li, C.-C. Chueh, H.-L. Yip, Z. Zhu and A. K. Y. Jen, *Nature Communications*, 2020, **11**, 177.
8. J. H. Heo, F. Zhang, J. K. Park, H. Joon Lee, D. S. Lee, S. J. Heo, J. M. Luther, J. J. Berry, K. Zhu and S. H. Im, *Joule*, 2022, **6**, 1672-1688.
9. T. Xu, W. Xiang, J. Yang, D. J. Kubicki, W. Tress, T. Chen, Z. Fang, Y. Liu and S. Liu, *Advanced Materials*, 2023, **35**, 2303346.
10. S. Wang, P. Wang, B. Shi, C. Sun, H. Sun, S. Qi, Q. Huang, S. Xu, Y. Zhao and X. Zhang, *Advanced Materials*, 2023, **35**, 2300581.
11. S. Fu, N. Sun, J. Le, W. Zhang, R. Miao, W. Zhang, Y. Kuang, W. Song and J. Fang, *ACS Applied Materials & Interfaces*, 2022, **14**, 30937-30945.
12. H. Sun, S. Wang, S. Qi, P. Wang, R. Li, B. Shi, Q. Zhang, Q. Huang, S. Xu, Y. Zhao and X. Zhang, *Advanced Functional Materials*, 2023, **33**, 2213913.
13. S. Fu, X. Li, J. Wan, W. Zhang, W. Song and J. Fang, *Advanced Functional Materials*, 2022, **32**, 2111116.
14. C. Lu, X. Li, X. Guo, S. Fu, W. Zhang, H. Yuan and J. Fang, *Chemical Engineering Journal*, 2023, **452**, 139495.
15. S. Fu, W. Zhang, X. Li, J. Guan, W. Song and J. Fang, *ACS Energy Letters*, 2021, **6**, 3661-3668.
16. C. Lu, X. Li, H. Yuan, W. Zhang, X. Guo, A. Liu, H. Yang, W. Li, Z. Cui, Y. Hu and J. Fang, *Chemical Engineering Journal*, 2024, **480**, 147267.
17. T. Xu, W. Xiang, X. Ru, Z. Wang, Y. Liu, N. Li, H. Xu and S. Liu, *Advanced Materials*, 2024, **36**, 2312237.
18. H. Sun, S. Wang, P. Wang, Y. Liu, S. Qi, B. Shi, Y. Zhao and X. Zhang, *Journal of Energy Chemistry*, 2025, **100**, 87-93.
19. J. H. Heo, J. K. Park, H. J. Lee, E. H. Shin, S. Y. Hong, K.-H. Hong, F. Zhang and S. H. Im, 2024, **36**, 2408387.
20. S. Wang, S. Qi, H. Sun, P. Wang, Y. Zhao and X. Zhang, *Angewandte Chemie International Edition*, 2024, **63**, e202400018.
21. D. Xu, M. Wu, Y. Bai, B. Wang, H. Zhou, Z. Fan, N. Zhang, J. Tan, H. Li, H. Bian and Z. Liu, *Advanced Functional Materials*, **n/a**, 2412946.
22. Z. Wang, T. Xu, N. Li, Y. Liu, K. Li, Z. Fan, J. Tan, D. Chen, S. Liu and W. Xiang, *Energy & Environmental Science*, 2024, **17**, 7271-7280.